MATCH
Communications in Mathematical and in Computer Chemistry

MATCH Commun. Math. Comput. Chem. **97** (2027) 1107–1137
ISSN: 0340–6253
doi: 10.46793/match.97-3.26826

A Regularized Volterra–Fredholm Integral Approach for the Two-Dimensional Brusselator System and Turing Pattern Simulation

Djihane Bouressace, Ridha Dida, Hamza Guebbai*

Laboratoire de Mathématiques Appliquées et de Modélisation, Université 8 Mai 1945 Guelma, B.P. 401, Guelma, 24000, Algeria

jihanebourssace@gmail.com; bouressace.djihane@univ-guelma.dz,
didarida25@yahoo.fr; dida.ridha@univ-guelma.dz,
guebaihamza@yahoo.fr; guebbai.hamza@univ-guelma.dz

(Received August 26, 2026)

Abstract

In this paper, we propose a regularized integral approach for the two-dimensional Brusselator reaction–diffusion system posed on the unit disk. The nonlinear source terms are first extended and regularized by convolution with a compactly supported mollifier, which naturally leads to an enlarged computational domain $B_\varepsilon = B(0, 1+\varepsilon)$. Using Duhamel's principle and the heat kernel, the original reaction–diffusion problem is transformed into a nonlinear Volterra–Fredholm integral system. We establish local Lipschitz estimates for the associated nonlinear integral operators in a suitable Banach space and prove the local existence and uniqueness of the regularized solution by a fixed-point argument. For the numerical approximation, a Nyström-type scheme is developed by applying quadrature rules simultaneously to the Volterra time integral and to the Fredholm spatial integral. Since the spatial domain is circular, the discretization

*Corresponding author.

is performed in polar coordinates. Numerical experiments are carried out with spatially heterogeneous input and output source terms, combining radial feed gradients and small stochastic perturbations. The simulations show the emergence of clear Turing-type patterns, characterized by localized activator peaks and complementary inhibitor distributions. Compared with standard finite-difference simulations of Brusselator-type models, the present integral formulation produces sharper and more clearly separated spatial structures.

1 Introduction

Reaction–diffusion systems constitute a fundamental class of mathematical models for describing the interaction between local nonlinear reactions and spatial diffusion. Such systems arise naturally in chemistry, biology, ecology, and physics, where they are used to model oscillations, wave propagation, and the emergence of spatially organized structures [4,5,7,10–12,14]. Since the pioneering work of Turing on morphogenesis [14], reaction–diffusion equations have played a central role in the mathematical explanation of pattern formation. Among the classical models in this field, the Brusselator system occupies a particularly important position.

The Brusselator model was introduced by Prigogine and Lefever [11] as a theoretical model for autocatalytic chemical reactions exhibiting oscillatory behavior and symmetry-breaking phenomena. It describes the evolution of two interacting chemical species, usually interpreted as an activator and an inhibitor. Despite its simple algebraic structure, the Brusselator system is able to reproduce a rich variety of dynamical regimes, including stable equilibria, temporal oscillations, traveling waves, and diffusion-driven Turing patterns. For this reason, it has become a paradigmatic model in the study of nonlinear chemical dynamics and pattern formation.

In its classical form, the Brusselator system is governed by reaction terms of cubic type coupled with diffusion. The nonlinear term X^2Y is responsible for the autocatalytic amplification of the activator, while the inhibitor component regulates the spatial growth through diffusion. When the inhibitor diffuses faster than the activator, the homogeneous state may lose stability under the effect of diffusion, leading to the formation of nonhomogeneous spatial structures. This mechanism is the basis of the

well-known Turing instability.

Several analytical and numerical approaches have been developed to investigate the Brusselator system. Classical studies focus on stability analysis, bifurcation theory, and numerical approximation of the corresponding reaction–diffusion equations. More recently, fractional and nonlocal generalizations of the Brusselator model have attracted increasing attention, since they allow the incorporation of memory effects and anomalous diffusion. In this direction, Merikhi *et al.* [9] proposed a conformable fractional approach to the Brusselator system and transformed the model into a nonlinear Volterra-type integral equation. Their work established existence and uniqueness results and developed a numerical approximation based on the Nyström method [9]. This shows the relevance of integral formulations in the analysis and simulation of Brusselator-type dynamics.

Integral equations provide a powerful framework for treating evolution problems, especially when memory, cumulative effects, or nonlinear source terms are involved. As emphasized in the classical monograph of Linz [2,3,8,13], Volterra integral equations are naturally adapted to initial value problems because their causal structure reflects the dependence of the present state on the past history of the system. Moreover, numerical methods for Volterra equations, such as quadrature and Nyström-type schemes, provide stable and flexible tools for approximating nonlinear evolution problems. This makes the integral approach particularly suitable for reaction–diffusion systems, where nonlinear reactions and diffusion effects interact over both time and space.

The present work follows this integral point of view, but differs from previous fractional or one-dimensional approaches in several essential aspects. We study the classical two-dimensional Brusselator reaction–diffusion system in the unit disk

$$B_1 = \{x \in \mathbb{R}^2 : \mid x \mid < 1\},$$

under homogeneous Dirichlet boundary conditions. The main objective is to construct a rigorous Volterra–Fredholm integral formulation of the system and to use this formulation as the basis for both analytical and

numerical investigations.

Our approach begins with the heat equation associated with the diffusion operator. The nonlinear right-hand side is first extended by zero outside the unit disk and then regularized by convolution with a compactly supported mollifier J_ε. This regularization makes the source term sufficiently smooth in the space variable. Since the support of the mollified function is enlarged by the convolution, the natural computational and analytical domain becomes

$$B_\varepsilon = B(0, 1 + \varepsilon).$$

Using Duhamel's principle and the fundamental solution of the heat equation [6], the regularized Brusselator system is then reformulated as a nonlinear Volterra–Fredholm integral system over B_ε.

The analytical part of this work is based on the study of the nonlinear integral operators generated by the Brusselator reaction terms. We first introduce a suitable Banach space of continuous-in-time functions with values in $L^\infty(B_\varepsilon)$. Then we prove local Lipschitz estimates for the nonlinear operators on bounded subsets of this space. These estimates allow us to apply a fixed-point argument and to establish the local existence and uniqueness of the integral solution. The construction can be extended step by step in time as long as the solution remains bounded.

For the numerical approximation, we develop a Nyström-type method applied simultaneously to the Volterra time integral and to the Fredholm spatial integral. Since the domain is a disk, the spatial discretization is performed in polar coordinates. The trapezoidal rule is used for both time and space integrations, and the convolution with the mollifier is approximated by the same quadrature structure. This leads to a fully discrete numerical scheme adapted to the integral formulation.

Finally, numerical experiments are carried out in order to illustrate the emergence of Turing-type spatial patterns. To reproduce a more realistic open-reactor setting, the source terms J_{in} and J_{out} are chosen as spatially heterogeneous functions, combining radial feed gradients and small stochastic fluctuations. This choice is motivated by experimental configu-

rations such as continuous-fed unstirred reactors, where chemical species are supplied through the boundary and microscopic imperfections naturally perturb the medium. The simulations show the transition from an initially almost homogeneous state to a stable nonhomogeneous configuration characterized by localized activator peaks and complementary inhibitor distributions.

The main contributions of this paper can be summarized as follows:

- We derive a Volterra–Fredholm integral formulation for the two-dimensional Brusselator system in a disk using mollification and Duhamel's principle.
- We justify the passage from the unit disk B_0 to the enlarged disk $B_\varepsilon = B(0, 1+\varepsilon)$ through the support property of the convolution kernel.
- We prove local Lipschitz continuity of the nonlinear integral operators and establish existence and uniqueness of the regularized integral solution.
- We construct a Nyström-type numerical scheme in polar coordinates for the approximation of both the Volterra and Fredholm integrals.
- We provide numerical simulations showing the formation of Turing-type patterns under spatially heterogeneous input and output source terms.

It is also worth comparing the present numerical patterns with those obtained in recent fractional Brusselator simulations based on finite difference schemes [1]. In such studies, the numerical results often display spatial variations, surface deformations, or contour structures generated by the fractional orders, but the resulting patterns may remain relatively diffuse or globally distributed over the computational domain. In contrast, the present Volterra–Fredholm integral approach, combined with a polar Nyström discretization and heterogeneous source terms, produces clearly separated and well-localized spatial structures.

More precisely, the patterns displayed in our approach are sharper and more visually distinct. The activator concentration X develops isolated

high-intensity spots arranged in a coherent circular configuration, while the inhibitor concentration Y exhibits complementary low-intensity regions at the same locations. This clear spatial separation between activator peaks and inhibitor valleys provides a more direct visualization of the Turing mechanism. The use of identical color scales for X and Y at each time level further reinforces this comparison and avoids artificial visual amplification of one component over the other.

This improvement in pattern clarity can be attributed to two main modeling choices. First, the radial geometry of the disk is well adapted to the emergence of annular and spot-like structures. Second, the spatially heterogeneous source terms J_{in} and J_{out}, constructed from radial gradients and small stochastic fluctuations, provide a physically motivated symmetry-breaking mechanism. As a consequence, the numerical solution evolves from an almost homogeneous state toward a stable configuration of localized spots, making the pattern formation process more explicit than in simulations where the source terms are spatially uniform or where the computational setting does not favor such localization.

From a chemical point of view, the spatial heterogeneity of the input and output source terms can be interpreted as a simplified description of nonuniform feeding and removal mechanisms in an open reactor. This makes the proposed model relevant not only as a mathematical regularization of the Brusselator system, but also as a numerical framework for reproducing experimentally meaningful chemical patterns.

The remainder of this paper is organized as follows. Section 2 presents the integral modeling of the two-dimensional Brusselator system, including the regularization procedure and the use of Duhamel's principle. Section 3 is devoted to the analytical study, where Lipschitz estimates and existence–uniqueness results are established. Section 4 describes the numerical discretization of the integral system using the Nyström method. Section 5 presents the numerical experiments and the parameter setting. Section 6 discusses the obtained Turing patterns and their interpretation. Finally, the paper ends with concluding remarks and possible perspectives.

2 Integral modeling of the two-dimensional Brusselator system

Let

$$B_0 = \left\{x \in \mathbb{R}^2 : \mid x \mid < 1\right\}$$

be the unit disk. We consider the two-dimensional Brusselator reaction–diffusion system

$$\begin{cases} \partial_t X - D_X \Delta X = J_{\text{in}} + \lambda_1 X^2 Y - (\lambda_2 + J_{\text{out}})X, & x \in B_0,\ t > 0, \\ \partial_t Y - D_Y \Delta Y = -\lambda_1 X^2 Y + \lambda_2 X, & x \in B_0,\ t > 0, \\ X(x,0) = 0, \qquad Y(x,0) = 0, & x \in B_0, \\ X(x,t) = Y(x,t) = 0, & x \in \partial B_0,\ t > 0. \end{cases} \tag{2.1}$$

Here $X = X(x,t)$ and $Y = Y(x,t)$ denote the concentrations of the two chemical species, $D_X, D_Y > 0$ are diffusion coefficients, $\lambda_1, \lambda_2 > 0$ are reaction parameters, while J_{in} and J_{out} represent, respectively, the input and output terms of the chemical process. The nonlinear reaction terms are given by

$$f_1(X,Y) = J_{\text{in}} + \lambda_1 X^2 Y - (\lambda_2 + J_{\text{out}})X, \tag{2.2}$$

and

$$f_2(X,Y) = -\lambda_1 X^2 Y + \lambda_2 X. \tag{2.3}$$

Thus, system (2.1) may be written in the compact form

$$\partial_t X - D_X \Delta X = f_1(X,Y), \qquad \partial_t Y - D_Y \Delta Y = f_2(X,Y). \tag{2.4}$$

The purpose of the present section is to derive an integral formulation of (2.1). The main idea is to regularize the right-hand sides by convolution in the space variable and then apply Duhamel's principle to the corresponding heat equations. This procedure allows us to obtain a Volterra–Fredholm integral representation of the Brusselator system.

Let f be a function defined on $B_0 \times [0,T]$. We denote by $\widetilde{f}$ its extension

by zero to the whole space $\mathbb{R}^2$, namely

$$\widetilde{f}(x,t) = \begin{cases} f(x,t), & x \in B_0,\ 0 \le t \le T, \\ 0, & x \in \mathbb{R}^2 \setminus B_0,\ 0 \le t \le T. \end{cases} \tag{2.5}$$

Let $J \in C_c^2(\mathbb{R}^2)$ be a nonnegative mollifier satisfying

$$\operatorname{supp} J \subset B(0,1), \qquad J(x) \ge 0, \qquad \int_{\mathbb{R}^2} J(x)\,dx = 1. \tag{2.6}$$

For example, one may take

$$J(x) = \begin{cases} C \exp\left(\dfrac{1}{|\,x\,|^2 - 1}\right), & |\,x\,| < 1, \\ 0, & |\,x\,| \ge 1, \end{cases} \tag{2.7}$$

where $C > 0$ is chosen such that

$$\int_{\mathbb{R}^2} J(x)\,dx = 1. \tag{2.8}$$

This function belongs to $C_c^\infty(\mathbb{R}^2)$, is nonnegative, and is supported in $B(0,1)$.

For $\varepsilon > 0$, we define

$$J_\varepsilon(x) = \frac{1}{\varepsilon^2} J\left(\frac{x}{\varepsilon}\right), \tag{2.9}$$

so that

$$\operatorname{supp} J_\varepsilon \subset B(0,\varepsilon), \qquad \int_{\mathbb{R}^2} J_\varepsilon(x)\,dx = 1. \tag{2.10}$$

The regularized version of f is then defined by

$$f_\varepsilon(x,t) = (J_\varepsilon * \widetilde{f})(x,t) = \int_{\mathbb{R}^2} J_\varepsilon(x-z)\widetilde{f}(z,t)\,dz. \tag{2.11}$$

Since $J_\varepsilon \in C_c^2(\mathbb{R}^2)$, the function f_ε is C^2 with respect to the space variable. Moreover, since $\widetilde{f}$ is supported in B_0 and J_ε is supported in $B(0,\varepsilon)$, one

has

$$\operatorname{supp} f_\varepsilon(\cdot,t) \subset B(0,1+\varepsilon), \qquad 0 \le t \le T. \tag{2.12}$$

This is the reason why the regularized integral formulation is naturally written on the enlarged disk

$$B_\varepsilon := B(0,1+\varepsilon). \tag{2.13}$$

The original physical problem is posed in B_0, but the convolution procedure enlarges the spatial support of the regularized source terms. Consequently, the integration domain becomes B_ε, and the solution in the original disk is recovered by restriction to B_0.

We now recall the fundamental solution of the heat equation. For $D > 0$, let

$$\Phi_D(x,t) = \begin{cases} \dfrac{1}{(4\pi D t)^{n/2}} \exp\left(-\dfrac{|\,x\,|^2}{4Dt}\right), & t > 0, \\ 0, & t < 0. \end{cases} \tag{2.14}$$

In dimension $n = 2$, this becomes

$$\Phi_D(x,t) = \begin{cases} \dfrac{1}{4\pi D t} \exp\left(-\dfrac{|\,x\,|^2}{4Dt}\right), & t > 0, \\ 0, & t < 0. \end{cases} \tag{2.15}$$

The function Φ_D is the fundamental solution associated with the operator

$$\partial_t - D\Delta.$$

According to Duhamel's principle for the nonhomogeneous heat equation, if

$$\partial_t u - D\Delta u = f(x,t), \qquad u(x,0) = 0, \tag{2.16}$$

then the solution is represented by

$$u(x,t) = \int_0^t \int_{\mathbb{R}^n} \Phi_D(x-y, t-s) f(y,s)\, dy\, ds. \tag{2.17}$$

This is precisely the representation formula given in Evans [**?**, Chapter 2, Section 3, formula (13)] for the nonhomogeneous heat equation, written here with the diffusion coefficient D.

In the present work, the source terms are first extended by zero and then regularized by convolution. Since their supports are contained in B_ε, formula (2.17) gives

$$u(x,t) = \int_0^t \int_{B_\varepsilon} \Phi_D(x-y, t-s) f_\varepsilon(y,s)\, dy\, ds. \tag{2.18}$$

Therefore, in our regularized model, the heat kernel is obtained directly from the fundamental solution Φ_D, and the effective spatial integration domain is B_ε.

Applying (2.18) to the first equation of the Brusselator system, with $D = D_X$, gives

$$X(x,t) = \int_0^t \int_{B_\varepsilon} \Phi_{D_X}(x-y, t-s) \left[J_\varepsilon * \left(J_{\text{in}} + \lambda_1 X^2 Y - (\lambda_2 + J_{\text{out}}) X \right) \right](y,s)\, dy\, ds. \tag{2.19}$$

Similarly, applying (2.18) to the second equation, with $D = D_Y$, gives

$$Y(x,t) = \int_0^t \int_{B_\varepsilon} \Phi_{D_Y}(x-y, t-s) \left[J_\varepsilon * \left(-\lambda_1 X^2 Y + \lambda_2 X \right) \right](y,s)\, dy\, ds. \tag{2.20}$$

Equations (2.19)–(2.20) constitute the regularized integral formulation of the two-dimensional Brusselator system. The time integral is of Volterra type, whereas the spatial integral is of Fredholm type. Hence, the Brusselator system is transformed into a nonlinear Volterra–Fredholm integral system.

It is useful for the subsequent analysis to separate the external input term J_{in} from the nonlinear reaction terms. We define

$$F(x,t) = \int_0^t \int_{B_\varepsilon} \Phi_{D_X}(x-y, t-s) \left(J_\varepsilon * J_{\text{in}} \right)(y,s)\, dy\, ds. \tag{2.21}$$

Then, for (X, Y), we introduce the nonlinear integral operators

$$N_1(X,Y)(x,t,s) = \int_{B_\varepsilon} \Phi_{D_X}(x-y, t-s) \left[J_\varepsilon * \left(\lambda_1 X^2 Y - (\lambda_2 + J_{\text{out}}) X \right) \right](y,s)\, dy, \tag{2.22}$$

and

$$N_2(X,Y)(x,t,s) = \int_{B_\varepsilon} \Phi_{D_Y}(x-y, t-s) \left[J_\varepsilon * \left(-\lambda_1 X^2 Y + \lambda_2 X \right) \right](y,s)\, dy. \tag{2.23}$$

With these definitions, the regularized Brusselator system takes the integral form

$$X(x,t) = F(x,t) + \int_0^t N_1(X,Y)(x,t,s)\, ds, \tag{2.24}$$

and

$$Y(x,t) = \int_0^t N_2(X,Y)(x,t,s)\, ds. \tag{2.25}$$

This formulation is the starting point of the analytical study. The convolution with J_ε provides the regularity required to apply Duhamel's principle, while the passage from B_0 to $B_\varepsilon = B(0, 1+\varepsilon)$ follows from the support property of the mollifier. Thus, the nonlinear Brusselator system is embedded into an integral framework based on the fundamental solution of the heat equation.

3 Analytical study

We now establish the analytical framework associated with the integral formulation obtained in the previous section. Throughout this section, we set

$$B_\varepsilon := B(0, 1+\varepsilon)$$

and

$$Q_T := B_\varepsilon \times [0, T].$$

We assume that

$$J_{\text{in}}, J_{\text{out}} \in L^\infty(Q_T), \qquad D_X, D_Y > 0, \qquad \lambda_1, \lambda_2 > 0.$$

Let

$$\mathcal{F} := L^\infty(B_\varepsilon)$$

be equipped with the norm

$$|| \, u \, ||_{\mathcal{F}} := \operatorname*{ess\,sup}_{x \in B_\varepsilon} \mid u(x) \mid .$$

For $T > 0$, we introduce the Banach space

$$\mathcal{E}_T := C([0,T]; \mathcal{F}) \times C([0,T]; \mathcal{F}),$$

endowed with the norm

$$|| \, (X,Y) \, ||_{\mathcal{E}_T} := \sup_{t \in [0,T]} || \, X(\cdot,t) \, ||_{\mathcal{F}} + \sup_{t \in [0,T]} || \, Y(\cdot,t) \, ||_{\mathcal{F}} .$$

For $R > 0$, we define the closed ball

$$\mathcal{B}_R := \{(X,Y) \in \mathcal{E}_T : || \, (X,Y) \, ||_{\mathcal{E}_T} \leq R\} .$$

In particular, if $(X,Y) \in \mathcal{B}_R$, then

$$|| \, X(\cdot,t) \, ||_{\mathcal{F}} \leq R, \qquad || \, Y(\cdot,t) \, ||_{\mathcal{F}} \leq R, \qquad 0 \leq t \leq T.$$

We shall use two elementary properties. First, since J_ε is nonnegative and has unit mass, convolution by J_ε is nonexpansive in L^∞, namely

$$|| \, J_\varepsilon * h \, ||_{\mathcal{F}} \leq || \, h \, ||_{\mathcal{F}} .$$

Second, for the heat kernel

$$\Phi_D(x,t) = \frac{1}{4\pi D t} \exp\left(-\frac{| \, x \, |^2}{4Dt} \right), \qquad t > 0,$$

one has, for every $x \in B_\varepsilon$ and $t > s$,

$$\int_{B_\varepsilon} \Phi_D(x-y, t-s)\, dy \leq \int_{\mathbb{R}^2} \Phi_D(x-y, t-s)\, dy = 1.$$

These two estimates are the main tools in the Lipschitz analysis of the nonlinear integral operators.

Theorem 1. *Let $R > 0$. The nonlinear integral operators N_1 and N_2, defined by*

$$N_1(X,Y)(x,t,s) = \int_{B_\varepsilon} \Phi_{D_X}(x-y, t-s) \left[J_\varepsilon * \left(\lambda_1 X^2 Y - (\lambda_2 + J_{\text{out}}) X \right) \right](y,s)\, dy,$$

and

$$N_2(X,Y)(x,t,s) = \int_{B_\varepsilon} \Phi_{D_Y}(x-y, t-s) \left[J_\varepsilon * \left(-\lambda_1 X^2 Y + \lambda_2 X \right) \right](y,s)\, dy,$$

are locally Lipschitz continuous on $\mathcal{B}_R$. More precisely, for every

$$(X_1, Y_1), (X_2, Y_2) \in \mathcal{B}_R$$

and for every $0 \leq s < t \leq T$, one has

$$\begin{aligned} &|| N_1(X_1,Y_1)(\cdot,t,s) - N_1(X_2,Y_2)(\cdot,t,s) ||_{\mathcal{F}} \\ &\quad \leq L_1(R) \left(|| X_1(\cdot,s) - X_2(\cdot,s) ||_{\mathcal{F}} + || Y_1(\cdot,s) - Y_2(\cdot,s) ||_{\mathcal{F}} \right), \end{aligned}$$

where

$$L_1(R) = 3\lambda_1 R^2 + \lambda_2 + || J_{\text{out}} ||_{L^\infty(Q_T)}.$$

Similarly,

$$\begin{aligned} &|| N_2(X_1,Y_1)(\cdot,t,s) - N_2(X_2,Y_2)(\cdot,t,s) ||_{\mathcal{F}} \\ &\quad \leq L_2(R) \left(|| X_1(\cdot,s) - X_2(\cdot,s) ||_{\mathcal{F}} + || Y_1(\cdot,s) - Y_2(\cdot,s) ||_{\mathcal{F}} \right), \end{aligned}$$

where

$$L_2(R) = 3\lambda_1 R^2 + \lambda_2.$$

Proof. Let

$$(X_1, Y_1), (X_2, Y_2) \in \mathcal{B}_R.$$

We set

$$\Delta X := X_1 - X_2, \qquad \Delta Y := Y_1 - Y_2.$$

The only nonlinear term to estimate is the cubic reaction term. We write

$$X_1^2 Y_1 - X_2^2 Y_2 = (X_1^2 - X_2^2) Y_1 + X_2^2 (Y_1 - Y_2).$$

Since

$$X_1^2 - X_2^2 = (X_1 - X_2)(X_1 + X_2),$$

we obtain

$$X_1^2 Y_1 - X_2^2 Y_2 = \Delta X (X_1 + X_2) Y_1 + X_2^2 \Delta Y.$$

Because $(X_i, Y_i) \in \mathcal{B}_R$, $i = 1, 2$, we have

$$| X_i(x,t) | \leq R, \qquad | Y_i(x,t) | \leq R$$

for almost every $x \in B_\varepsilon$ and every $t \in [0, T]$. Hence

$$| X_1 + X_2 | \leq 2R, \qquad | Y_1 | \leq R, \qquad | X_2 |^2 \leq R^2.$$

Therefore,

$$| X_1^2 Y_1 - X_2^2 Y_2 | \leq 2R^2 | \Delta X | + R^2 | \Delta Y | .$$

It follows that

$$|| X_1^2 Y_1 - X_2^2 Y_2 ||_{\mathcal{F}} \leq 2R^2 || \Delta X(\cdot, s) ||_{\mathcal{F}} + R^2 || \Delta Y(\cdot, s) ||_{\mathcal{F}} .$$

We now estimate N_1. For $0 \leq s < t \leq T$, one has

$$\begin{aligned} &N_1(X_1, Y_1)(x,t,s) - N_1(X_2, Y_2)(x,t,s) \\ &= \int_{B_\varepsilon} \Phi_{D_X}(x - y, t - s) \left[J_\varepsilon * \left(\lambda_1 (X_1^2 Y_1 - X_2^2 Y_2) \right.\right. \\ &\qquad \left.\left. - (\lambda_2 + J_{\text{out}})(X_1 - X_2) \right) \right] (y, s)\, dy. \end{aligned}$$

Using the positivity of the heat kernel, the fact that its integral over B_ε is bounded by 1, and the L^∞-stability of the convolution, we get

$$\begin{aligned}&|| N_1(X_1,Y_1)(\cdot,t,s) - N_1(X_2,Y_2)(\cdot,t,s) ||_{\mathcal{F}}\\ &\le \lambda_1 || X_1^2Y_1 - X_2^2Y_2 ||_{\mathcal{F}} + \left(\lambda_2 + || J_{\text{out}} ||_{L^\infty(Q_T)}\right) || \Delta X(\cdot,s) ||_{\mathcal{F}} .\end{aligned}$$

Consequently,

$$\begin{aligned}&|| N_1(X_1,Y_1)(\cdot,t,s) - N_1(X_2,Y_2)(\cdot,t,s) ||_{\mathcal{F}}\\ &\le \left(2\lambda_1R^2 + \lambda_2 + || J_{\text{out}} ||_{L^\infty(Q_T)}\right) || \Delta X(\cdot,s) ||_{\mathcal{F}} + \lambda_1R^2 || \Delta Y(\cdot,s) ||_{\mathcal{F}} .\end{aligned}$$

Thus,

$$\begin{aligned}&|| N_1(X_1,Y_1)(\cdot,t,s) - N_1(X_2,Y_2)(\cdot,t,s) ||_{\mathcal{F}}\\ &\le \left(3\lambda_1R^2 + \lambda_2 + || J_{\text{out}} ||_{L^\infty(Q_T)}\right) \left(|| \Delta X(\cdot,s) ||_{\mathcal{F}} + || \Delta Y(\cdot,s) ||_{\mathcal{F}}\right).\end{aligned}$$

This proves the Lipschitz estimate for N_1.

For N_2, we similarly write

$$\begin{aligned}&N_2(X_1,Y_1)(x,t,s) - N_2(X_2,Y_2)(x,t,s)\\ &= \int_{B_\varepsilon} \Phi_{D_Y}(x-y,t-s)\left[J_\varepsilon * \left(-\lambda_1(X_1^2Y_1 - X_2^2Y_2)\right.\right.\\ &\qquad \left.\left. + \lambda_2(X_1 - X_2)\right)\right](y,s)\,dy.\end{aligned}$$

Using the same estimates, we obtain

$$\begin{aligned}&|| N_2(X_1,Y_1)(\cdot,t,s) - N_2(X_2,Y_2)(\cdot,t,s) ||_{\mathcal{F}}\\ &\le \lambda_1 || X_1^2Y_1 - X_2^2Y_2 ||_{\mathcal{F}} + \lambda_2 || \Delta X(\cdot,s) ||_{\mathcal{F}}\\ &\le (2\lambda_1R^2 + \lambda_2) || \Delta X(\cdot,s) ||_{\mathcal{F}} + \lambda_1R^2 || \Delta Y(\cdot,s) ||_{\mathcal{F}} .\end{aligned}$$

Hence

$$\begin{aligned}&|| N_2(X_1,Y_1)(\cdot,t,s) - N_2(X_2,Y_2)(\cdot,t,s) ||_{\mathcal{F}}\\ &\le (3\lambda_1R^2 + \lambda_2)\left(|| \Delta X(\cdot,s) ||_{\mathcal{F}} + || \Delta Y(\cdot,s) ||_{\mathcal{F}}\right).\end{aligned}$$

The proof is complete. ■

We now use the preceding Lipschitz estimates to prove existence and

uniqueness of a solution to the regularized integral system. Let

$$F_0(x,t) = \int_0^t \int_{B_\varepsilon} \Phi_{D_X}(x-y, t-s)\,(J_\varepsilon * J_{\text{in}})\,(y,s)\,dy\,ds.$$

The integral formulation can be written as

$$X(x,t) = F_0(x,t) + \int_0^t N_1(X,Y)(x,t,s)\,ds,$$

$$Y(x,t) = \int_0^t N_2(X,Y)(x,t,s)\,ds.$$

We define the operator

$$\mathcal{T} : \mathcal{E}_\tau \longrightarrow \mathcal{E}_\tau$$

by

$$\mathcal{T}(X,Y) = (\mathcal{T}_1(X,Y), \mathcal{T}_2(X,Y)),$$

where, for $0 \le t \le \tau$,

$$\mathcal{T}_1(X,Y)(x,t) = F_0(x,t) + \int_0^t N_1(X,Y)(x,t,s)\,ds,$$

and

$$\mathcal{T}_2(X,Y)(x,t) = \int_0^t N_2(X,Y)(x,t,s)\,ds.$$

Theorem 2. *Assume that*

$$J_{\text{in}}, J_{\text{out}} \in L^\infty(Q_T).$$

Then there exists $\tau \in (0,T]$ *such that the regularized Volterra–Fredholm system*

$$X(x,t) = F_0(x,t) + \int_0^t N_1(X,Y)(x,t,s)\,ds,$$

$$Y(x,t) = \int_0^t N_2(X,Y)(x,t,s)\,ds$$

admits a unique solution

$$(X,Y) \in \mathcal{E}_\tau.$$

Moreover, this solution is obtained as the limit in $\mathcal{E}_\tau$ of the Picard iteration

$$X_{n+1}(x,t) = F_0(x,t) + \int_0^t N_1(X_n, Y_n)(x,t,s)\, ds,$$

$$Y_{n+1}(x,t) = \int_0^t N_2(X_n, Y_n)(x,t,s)\, ds,$$

starting for instance from

$$X_0(x,t) = F_0(x,t), \qquad Y_0(x,t) = 0.$$

Proof. Let $R > 0$ be fixed and consider the closed ball

$$\mathcal{B}_R^\tau := \{(X,Y) \in \mathcal{E}_\tau : || \, (X,Y) \, ||_{\mathcal{E}_\tau} \leq R\}.$$

Since $F_0(\cdot, 0) = 0$ and $F_0 \in C([0,T]; \mathcal{F})$, we have

$$A_\tau := \sup_{t\in[0,\tau]} || \, F_0(\cdot,t) \, ||_{\mathcal{F}} \longrightarrow 0 \qquad \text{as } \tau \to 0^+.$$

Let $(X,Y) \in \mathcal{B}_R^\tau$. Using the positivity of the heat kernel, the bound

$$\int_{B_\varepsilon} \Phi_D(x-y, t-s)\, dy \leq 1,$$

and the L^∞-stability of the mollifier, we obtain

$$|| \, N_1(X,Y)(\cdot,t,s) \, ||_{\mathcal{F}} \leq \lambda_1 R^3 + \left(\lambda_2 + || \, J_{\text{out}} \, ||_{L^\infty(Q_T)}\right) R,$$

and

$$|| \, N_2(X,Y)(\cdot,t,s) \, ||_{\mathcal{F}} \leq \lambda_1 R^3 + \lambda_2 R.$$

Therefore,

$$\begin{aligned} || \, \mathcal{T}(X,Y) \, ||_{\mathcal{E}_\tau} \leq A_\tau &+ \tau \left[\lambda_1 R^3 + \left(\lambda_2 + || \, J_{\text{out}} \, ||_{L^\infty(Q_T)}\right) R\right] \\ &+ \tau \left[\lambda_1 R^3 + \lambda_2 R\right]. \end{aligned}$$

Thus

$$|| \mathcal{T}(X,Y) ||_{\mathcal{E}_\tau} \leq A_\tau + \tau \left[2\lambda_1 R^3 + \left(2\lambda_2 + || J_{\text{out}} ||_{L^\infty(Q_T)}\right) R\right].$$

Since $A_\tau \to 0$ as $\tau \to 0^+$, we may choose $\tau > 0$ sufficiently small such that

$$A_\tau + \tau \left[2\lambda_1 R^3 + \left(2\lambda_2 + || J_{\text{out}} ||_{L^\infty(Q_T)}\right) R\right] \leq R.$$

Hence

$$\mathcal{T}(\mathcal{B}_R^\tau) \subset \mathcal{B}_R^\tau.$$

We now prove that $\mathcal{T}$ is a contraction on $\mathcal{B}_R^\tau$. Let

$$(X_1, Y_1), (X_2, Y_2) \in \mathcal{B}_R^\tau.$$

By Theorem 1, for all $0 \leq s < t \leq \tau$,

$$\begin{aligned} &|| N_1(X_1,Y_1)(\cdot,t,s) - N_1(X_2,Y_2)(\cdot,t,s) ||_{\mathcal{F}} \\ &\quad \leq L_1(R) \left(|| X_1(\cdot,s) - X_2(\cdot,s) ||_{\mathcal{F}} + || Y_1(\cdot,s) - Y_2(\cdot,s) ||_{\mathcal{F}}\right), \end{aligned}$$

and

$$\begin{aligned} &|| N_2(X_1,Y_1)(\cdot,t,s) - N_2(X_2,Y_2)(\cdot,t,s) ||_{\mathcal{F}} \\ &\quad \leq L_2(R) \left(|| X_1(\cdot,s) - X_2(\cdot,s) ||_{\mathcal{F}} + || Y_1(\cdot,s) - Y_2(\cdot,s) ||_{\mathcal{F}}\right). \end{aligned}$$

Consequently,

$$\begin{aligned} &|| \mathcal{T}(X_1,Y_1) - \mathcal{T}(X_2,Y_2) ||_{\mathcal{E}_\tau} \\ &\quad \leq \tau \left(L_1(R) + L_2(R)\right) || (X_1 - X_2, Y_1 - Y_2) ||_{\mathcal{E}_\tau}. \end{aligned}$$

Choosing $\tau > 0$ even smaller if necessary, we can impose

$$\tau \left(L_1(R) + L_2(R)\right) < 1.$$

Therefore $\mathcal{T}$ is a contraction on the complete metric space $\mathcal{B}_R^\tau$. By the Banach fixed-point theorem, $\mathcal{T}$ admits a unique fixed point in $\mathcal{B}_R^\tau$. This

fixed point satisfies

$$X(x,t) = F_0(x,t) + \int_0^t N_1(X,Y)(x,t,s)\,ds,$$

and

$$Y(x,t) = \int_0^t N_2(X,Y)(x,t,s)\,ds.$$

Thus (X,Y) is a solution of the regularized integral Brusselator system on $[0,\tau]$.

The convergence of the Picard sequence follows directly from the contraction property. Indeed, if

$$(X_{n+1}, Y_{n+1}) = \mathcal{T}(X_n, Y_n),$$

then

$$|| \,(X_{n+1} - X_n, Y_{n+1} - Y_n)\, ||_{\mathcal{E}_\tau} \leq q \,|| \,(X_n - X_{n-1}, Y_n - Y_{n-1})\, ||_{\mathcal{E}_\tau},$$

where

$$q := \tau\,(L_1(R) + L_2(R)) < 1.$$

Hence (X_n, Y_n) is a Cauchy sequence in $\mathcal{E}_\tau$, and its limit is the unique fixed point of $\mathcal{T}$. The proof is complete. ■

The previous theorem gives local existence and uniqueness. By repeating the same argument on successive time intervals, the solution may be continued as long as its $\mathcal{E}_T$-norm remains bounded. More precisely, if the solution satisfies an a priori bound

$$\sup_{t\in[0,T]} (|| \,X(\cdot,t)\, ||_{\mathcal{F}} + || \,Y(\cdot,t)\, ||_{\mathcal{F}}) < +\infty,$$

then the local construction can be iterated finitely many times, and the solution is uniquely extended to the whole interval $[0,T]$.

4 Numerical discretization of the integral system

We now describe the numerical approximation of the regularized Volterra–Fredholm integral formulation of the two-dimensional Brusselator system. The method used is a Nyström-type discretization applied both to the Volterra time integral and to the Fredholm space integral. Since the spatial domain is the enlarged disk

$$B_\varepsilon = B(0, 1+\varepsilon),$$

it is natural to use polar coordinates. We set

$$R_\varepsilon := 1 + \varepsilon.$$

For $D > 0$, the heat kernel used in the integral formulation is

$$\Phi_D(x,t) = \begin{cases} \dfrac{1}{4\pi D t} \exp\left(-\dfrac{|\,x\,|^2}{4Dt}\right), & t > 0, \\ 0, & t = 0. \end{cases} \tag{4.1}$$

In the numerical scheme, the value at $t = 0$ is taken as

$$\Phi_D(x,0) = 0, \tag{4.2}$$

which corresponds to the continuous extension of the kernel for $x \neq 0$ and avoids the singularity at the diagonal time level in the quadrature formula.

We recall that the regularized Brusselator system is written as

$$\begin{aligned} X(x,t) = \int_0^t \int_{B_\varepsilon} \Phi_{D_X}(x-y, t-s) \big[J_\varepsilon * \big(J_{\mathrm{in}} + \lambda_1 X^2 Y \\ - (\lambda_2 + J_{\mathrm{out}}) X \big) \big] (y,s)\, dy\, ds, \end{aligned} \tag{4.3}$$

and

$$Y(x,t) = \int_0^t \int_{B_\varepsilon} \Phi_{D_Y}(x-y, t-s) \left[J_\varepsilon * \left(-\lambda_1 X^2 Y + \lambda_2 X \right) \right](y,s)\, dy\, ds. \tag{4.4}$$

The convolution kernel is chosen explicitly. We take

$$J(x_1,x_2) = \begin{cases} k\left(1-(x_1^2+x_2^2)^2\right)^2, & x_1^2+x_2^2<1, \\ 0, & x_1^2+x_2^2 \geq 1. \end{cases} \tag{4.5}$$

The constant k is determined from the normalization condition

$$\int_{\mathbb{R}^2} J(x)\, dx = 1.$$

Using polar coordinates, $x_1^2+x_2^2 = r^2$, we have

$$1 = k \int_0^{2\pi} \int_0^1 \left(1-r^4\right)^2 r\, dr\, d\theta. \tag{4.6}$$

Therefore,

$$\int_0^1 \left(1-r^4\right)^2 r\, dr = \int_0^1 \left(1-2r^4+r^8\right) r\, dr = \frac{1}{2} - \frac{1}{3} + \frac{1}{10} = \frac{4}{15}. \tag{4.7}$$

It follows that

$$\int_0^{2\pi} \int_0^1 \left(1-r^4\right)^2 r\, dr\, d\theta = 2\pi \frac{4}{15} = \frac{8\pi}{15}. \tag{4.8}$$

Hence

$$k = \frac{15}{8\pi}. \tag{4.9}$$

Consequently,

$$J(x_1,x_2) = \begin{cases} \dfrac{15}{8\pi}\left(1-(x_1^2+x_2^2)^2\right)^2, & x_1^2+x_2^2<1, \\ 0, & x_1^2+x_2^2 \geq 1. \end{cases} \tag{4.10}$$

For $\varepsilon > 0$, the scaled mollifier is

$$J_\varepsilon(x) = \frac{1}{\varepsilon^2} J\left(\frac{x}{\varepsilon}\right). \tag{4.11}$$

Equivalently,

$$J_\varepsilon(x_1, x_2) = \begin{cases} \dfrac{15}{8\pi\varepsilon^2}\left[1 - \left(\dfrac{x_1^2 + x_2^2}{\varepsilon^2}\right)^2\right]^2, & x_1^2 + x_2^2 < \varepsilon^2, \\ 0, & x_1^2 + x_2^2 \geq \varepsilon^2. \end{cases} \tag{4.12}$$

Let N_t, N_r, N_θ be positive integers. We discretize the time interval $[0, T]$ by

$$t_n = (n-1)\Delta t, \qquad \Delta t = \frac{T}{N_t - 1}, \qquad 1 \leq n \leq N_t. \tag{4.13}$$

The extended disk B_ε is discretized in polar coordinates by

$$r_i = (i-1)h_r, \qquad h_r = \frac{R_\varepsilon}{N_r - 1}, \qquad 1 \leq i \leq N_r, \tag{4.14}$$

and

$$\theta_j = (j-1)h_\theta, \qquad h_\theta = \frac{2\pi}{N_\theta - 1}, \qquad 1 \leq j \leq N_\theta. \tag{4.15}$$

The corresponding Cartesian grid points are

$$z_{ij} = (r_i \cos\theta_j, r_i \sin\theta_j). \tag{4.16}$$

The area element in polar coordinates is

$$dy = r\, dr\, d\theta. \tag{4.17}$$

Therefore, for a sufficiently regular function g, the Fredholm integral over B_ε is approximated by the trapezoidal rule

$$\int_{B_\varepsilon} g(y)\, dy = \int_0^{2\pi}\int_0^{R_\varepsilon} g(r,\theta) r\, dr\, d\theta \approx h_r h_\theta \sum_{i=1}^{N_r}\sum_{j=1}^{N_\theta} \omega_i^r \omega_j^\theta g(z_{ij}) r_i, \tag{4.18}$$

where

$$\omega_1^r = \omega_{N_r}^r = \frac{1}{2}, \qquad \omega_i^r = 1, \quad 2 \le i \le N_r - 1, \tag{4.19}$$

and

$$\omega_1^\theta = \omega_{N_\theta}^\theta = \frac{1}{2}, \qquad \omega_j^\theta = 1, \quad 2 \le j \le N_\theta - 1. \tag{4.20}$$

Similarly, the Volterra integral over $[0, t_n]$ is approximated by

$$\int_0^{t_n} q(s)\, ds \approx \Delta t \sum_{k=1}^{n} \omega_k^{t,n} q(t_k), \tag{4.21}$$

with

$$\omega_1^{t,n} = \omega_n^{t,n} = \frac{1}{2}, \qquad \omega_k^{t,n} = 1, \quad 2 \le k \le n - 1. \tag{4.22}$$

We denote the numerical approximations by

$$X_{ij}^n \approx X(z_{ij}, t_n), \qquad Y_{ij}^n \approx Y(z_{ij}, t_n). \tag{4.23}$$

At each time level t_k, we compute the nonlinear reaction terms directly over the entire computational domain B_ε to prevent boundary artifacts:

$$H_{1,pq}^k = J_{\text{in}}(z_{pq}, t_k) + \lambda_1 (X_{pq}^k)^2 Y_{pq}^k - (\lambda_2 + J_{\text{out}}(z_{pq}, t_k))\, X_{pq}^k, \tag{4.24}$$

and

$$H_{2,pq}^k = -\lambda_1 (X_{pq}^k)^2 Y_{pq}^k + \lambda_2 X_{pq}^k. \tag{4.25}$$

The discrete convolution by J_ε over the domain is then approximated by the same Nyström quadrature:

$$\mathcal{M}_\varepsilon[H_\ell]_{pq}^k = h_r h_\theta \sum_{a=1}^{N_r} \sum_{b=1}^{N_\theta} \omega_a^r \omega_b^\theta J_\varepsilon(z_{pq} - z_{ab}) H_{\ell,ab}^k r_a, \qquad \ell = 1, 2. \tag{4.26}$$

Thus,

$$\mathcal{M}_\varepsilon[H_\ell]_{pq}^k \approx (J_\varepsilon * H_\ell)\,(z_{pq}, t_k). \tag{4.27}$$

Applying the Nyström method to both the Volterra time integral and the Fredholm space integral in (4.3), we obtain, for $1 \le i \le N_r$, $1 \le j \le$

N_θ, and $1 \le n \le N_t$,

$$X_{ij}^n = \Delta t\, h_r h_\theta \sum_{k=1}^{n} \omega_k^{t,n} \sum_{p=1}^{N_r} \sum_{q=1}^{N_\theta} \omega_p^r \omega_q^\theta \Phi_{D_X}(z_{ij} - z_{pq}, t_n - t_k) \mathcal{M}_\varepsilon[H_1]_{pq}^k r_p. \tag{4.28}$$

Similarly, from (4.4), we obtain

$$Y_{ij}^n = \Delta t\, h_r h_\theta \sum_{k=1}^{n} \omega_k^{t,n} \sum_{p=1}^{N_r} \sum_{q=1}^{N_\theta} \omega_p^r \omega_q^\theta \Phi_{D_Y}(z_{ij} - z_{pq}, t_n - t_k) \mathcal{M}_\varepsilon[H_2]_{pq}^k r_p. \tag{4.29}$$

Because of the convention

$$\Phi_D(x, 0) = 0, \tag{4.30}$$

the terms corresponding to $k = n$ vanish in (4.28)–(4.29). Therefore, the approximation at time t_n depends only on the previous time levels $t_1, \ldots, t_{n-1}$. This yields a time-marching scheme consistent with the Volterra structure of the integral formulation.

The initial conditions are

$$X_{ij}^1 = 0, \qquad Y_{ij}^1 = 0, \qquad 1 \le i \le N_r, \quad 1 \le j \le N_\theta. \tag{4.31}$$

For $n \ge 2$, the values X_{ij}^n and Y_{ij}^n are computed successively from (4.28)–(4.29). The complete numerical scheme is therefore based on three ingredients: the polar discretization of the enlarged disk B_ε, the trapezoidal Nyström approximation of both the Volterra and Fredholm integrals, and the discrete convolution with the compactly supported mollifier J_ε. This provides a fully discrete approximation of the regularized two-dimensional Brusselator system.

5 Numerical experiments and parameter setting

In this section, we present the numerical experiments performed using the fully discrete Nyström scheme introduced in the previous section. The aim is to investigate the emergence of spatial patterns in the two-dimensional regularized Brusselator system posed on the enlarged disk

$$B_\varepsilon = B(0, 1+\varepsilon).$$

The computations are carried out in polar coordinates on the domain

$$B_\varepsilon = B(0, R_\varepsilon), \qquad R_\varepsilon = 1+\varepsilon.$$

The numerical values used in the simulation are chosen as follows:

$$D_X = 0.01, \qquad D_Y = 0.10, \tag{5.1}$$

$$\lambda_1 = 1.0, \qquad \lambda_2 = 4.0, \tag{5.2}$$

and

$$J_{\text{in}}^{(0)} = 2.0, \qquad J_{\text{out}}^{(0)} = 1.0. \tag{5.3}$$

The diffusion coefficient of the inhibitor Y is therefore ten times larger than that of the activator X. This choice is consistent with the classical activator–inhibitor mechanism responsible for Turing pattern formation.

The regularization parameter is taken as

$$\varepsilon = 0.20, \qquad R_\varepsilon = 1.20. \tag{5.4}$$

The final time and the time discretization are given by

$$T = 20.0, \qquad N_t = 500, \qquad \Delta t = \frac{T}{N_t - 1} = \frac{20}{499} \simeq 0.04008. \tag{5.5}$$

The spatial grid is defined by

$$N_r = 20, \qquad N_\theta = 40, \tag{5.6}$$

so that the total number of spatial grid points is

$$N_s = N_r N_\theta = 800. \tag{5.7}$$

In order to reproduce a more realistic experimental setting, the input and output source terms are not taken as spatially homogeneous constants. Instead, they are chosen as spatially heterogeneous functions inspired by open gel reactors, where the chemical species are continuously fed through the boundary. This produces macroscopic concentration gradients, while microscopic imperfections are modeled by stochastic fluctuations.

Let

$$r = \sqrt{x_1^2 + x_2^2}.$$

We define the input term by

$$J_{\text{in}}(x_1, x_2) = J_{\text{in}}^{(0)} \left[1 + \alpha_{\text{in}} \left(\frac{r}{R_\varepsilon} \right)^2 + \sigma_{\text{in}} \eta(x_1, x_2) \right], \tag{5.8}$$

and the output term by

$$J_{\text{out}}(x_1, x_2) = J_{\text{out}}^{(0)} \left[1 + \alpha_{\text{out}} \left(\frac{r}{R_\varepsilon} \right)^2 + \sigma_{\text{out}} \xi(x_1, x_2) \right]. \tag{5.9}$$

Here η and ξ are two independent random fields uniformly distributed in the interval $[-1, 1]$. In the numerical implementation, they are generated independently at the spatial grid points by

$$\eta_{ij} = 2\mathcal{R}_{ij}^{(1)} - 1, \qquad \xi_{ij} = 2\mathcal{R}_{ij}^{(2)} - 1, \tag{5.10}$$

where

$$\mathcal{R}_{ij}^{(1)}, \mathcal{R}_{ij}^{(2)} \sim \mathcal{U}(0, 1)$$

are independent uniformly distributed random variables. Thus,

$$\eta_{ij}, \xi_{ij} \sim \mathcal{U}(-1, 1).$$

The two random fields are generated once at the beginning of the simulation and remain fixed during the time evolution. Consequently, the source terms J_{in} and J_{out} are heterogeneous in space but constant in time. The fixed realization of η and ξ is not interpreted as a time-dependent stochastic forcing, but rather as a frozen spatial disorder representing small imperfections in the reactor or in the medium.

The parameters used in the simulation are

$$\alpha_{\text{in}} = 0.20, \qquad \alpha_{\text{out}} = 0.15, \tag{5.10}$$

and

$$\sigma_{\text{in}} = 0.05, \qquad \sigma_{\text{out}} = 0.05. \tag{5.11}$$

Thus, the input source has a 20% radial increase toward the boundary, while the output source has a 15% radial increase. The random fluctuations have amplitude 5% for both source terms.

The random fields are introduced in order to break the perfect radial symmetry of the disk and to initiate the instability. In the numerical implementation, a fixed random seed is used in order to make the simulation reproducible. These perturbations remain small compared with the deterministic radial gradients and therefore do not dominate the reaction–diffusion dynamics.

With these choices, the numerical experiment is designed to capture the transition from an initially almost homogeneous state to a nonhomogeneous spatial configuration generated by the interaction between nonlinear reaction kinetics and unequal diffusion rates.

6 Results and discussion

Figure 1 shows the evolution of the concentrations X and Y at six different time levels. The snapshots start at $t = \Delta t \simeq 0.04$, rather than at $t = 0$, in

order to avoid displaying the trivial initial condition. For each time level, the concentration X is displayed on the left and the concentration Y on the right, using the same color scale in order to allow a direct comparison between the two chemical species.

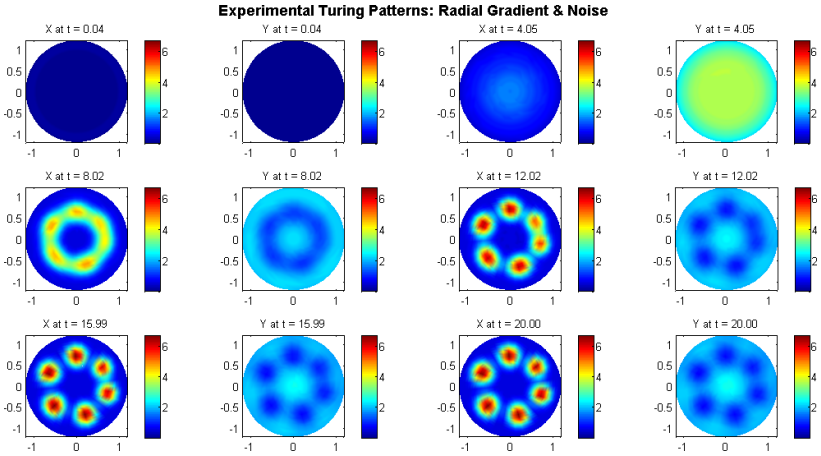

Figure 1. Numerical evolution of the two-dimensional Brusselator system in the enlarged disk $B_\varepsilon = B(0, 1.20)$. The left panel of each pair represents the activator concentration X, while the right panel represents the inhibitor concentration Y. The simulation is performed with $D_X = 0.01$, $D_Y = 0.10$, $\lambda_1 = 1.0$, $\lambda_2 = 4.0$, $J_{\text{in}}^{(0)} = 2.0$, $J_{\text{out}}^{(0)} = 1.0$, $\varepsilon = 0.20$, $T = 20.0$, $N_t = 500$, $N_r = 20$, and $N_\theta = 40$.

At the initial stage $t \simeq 0.04$, both concentrations remain almost homogeneous. This is consistent with the imposed initial conditions

$$X(x, 0) = 0, \qquad Y(x, 0) = 0,$$

and with the fact that the nonlinear interaction has not yet generated significant spatial organization.

At $t \simeq 4.05$, the effect of the radial feed terms becomes visible. The activator X starts to increase inside the disk, while the inhibitor Y develops a smoother and more diffuse spatial profile. This difference is due to the larger diffusion coefficient of Y, namely

$$D_Y = 0.10 > D_X = 0.01.$$

The inhibitor therefore spreads more rapidly than the activator.

At $t \simeq 8.02$, the spatial instability becomes clearly visible. The activator concentration X begins to form localized high-concentration regions arranged along an annular structure. This annular emergence is explained by the radial form of the source terms J_{in} and J_{out}, whose values increase toward the boundary. The random perturbations then break the radial symmetry and select localized spots.

For later times, especially at $t \simeq 12.02$, $t \simeq 15.99$, and $t = 20.00$, the system reaches a structured spatial regime. The activator X forms several intense localized spots, while the inhibitor Y presents lower concentration regions around the same locations. This opposite spatial behavior reflects the classical activator–inhibitor mechanism: regions where X is amplified are surrounded and regulated by the faster diffusion of Y.

The final pattern at $t = 20.00$ is stable and clearly nonhomogeneous. It consists of a circular arrangement of localized activator peaks, together with a complementary inhibitor distribution. This confirms that the regularized Volterra–Fredholm integral formulation, combined with the Nyström discretization, is able to reproduce the formation of Turing-type spatial patterns in the two-dimensional Brusselator system.

The numerical experiment also shows that the use of heterogeneous source terms is important. If J_{in} and J_{out} are taken as purely constant functions, the system may remain too symmetric and the formation of visible spatial patterns can be delayed or suppressed. In contrast, the radial gradients and small stochastic fluctuations used in (5.8)–(5.9) provide a realistic mechanism for triggering symmetry breaking, while preserving the underlying reaction–diffusion structure of the model.

Compared with the fractional Brusselator simulations reported in [1], where the patterns are mainly observed through smooth contour variations or surface deformations, the present simulations exhibit more clearly identifiable Turing structures. In particular, the activator X forms distinct localized spots, whereas the inhibitor Y develops a complementary distribution. This makes the spatial organization more readable and highlights more clearly the activator–inhibitor separation underlying the Turing mechanism.

References

[1] S. Ahmad, I. Ahmad, A. S. Alluhaidan, M. A. ElAffendi, M. Hleili, M. S. Alatawi, A theoretical and computational study of the fractional Brusselator system with neural network validation, *Sci. Rep.* **16** (2026) #18754 **doi:** 10.1038/s41598-026-47451-4.

[2] K. Atkinson, W. Han, *Theoretical Numerical Analysis: A Functional Analysis Approach*, Springer, New York, 2009, **doi:** 10.1007/978-1-4419-0458-4.

[3] H. Belhireche, H. Guebbai, On the mixed nonlinear integro-differential equations with weakly singular kernel, *Comput. Appl. Math.* **41** (2022) #36, **doi:** 10.1007/s40314-021-01743-9.

[4] J. Bisquert, L. Bertoluzzi, I. Mora-Seró, G. Garcia-Belmonte, Theory of impedance and capacitance spectroscopy of solar cells with dielectric relaxation, drift-diffusion transport, and recombination, *J. Phys. Chem. C* **118** (2014) 18983–18991, **doi:** 10.1021/jp5051644.

[5] D. G. Blackmond, Autocatalytic models for the origin of biological homochirality, *Chem. Rev.* **120** (2019) 4831–4847, **doi:** 10.1021/acs.chemrev.9b00557.

[6] L. C. Evans, *Partial Differential Equations*, AMS, Providence, 2010.

[7] R. M. Jena, S. Chakraverty, H. Rezazadeh, D. D. Ganji, On the solution of time-fractional dynamical model of Brusselator reaction-diffusion system arising in chemical reactions, *Math. Meth. Appl. Sci.* **43** (2020) 3903–3913, **doi:** 10.1002/mma.6157.

[8] P. Linz, *Analytical and Numerical Methods for Volterra Equations*, Soc. Industrial Appl. Math., Philadelphia, 1985.

[9] M. L. Merikhi, H. Guebbai, N. Benrabia, M. M. Bekkouche, A novel conformable fractional approach to the Brusselator system with numerical simulation, *J. Appl. Math. Comput.* **70** (2024) 1707–1721, **doi:** 10.1007/s12190-024-02022-6.

[10] J. D. Murray, *Mathematical Biology II: Spatial Models and Biomedical Applications*, Springer, New York, 2003, **doi:** 10.1007/b98869.

[11] I. Prigogine, R. Lefever, Symmetry breaking instabilities in dissipative systems. II, *J. Chem. Phys.* **48** (1968) 1695–1700, **doi:** 10.1063/1.1668896.

[12] S. Rüdiger, D. G. Míguez, A. P. Muñuzuri, F. Sagués, J. Casademunt, Dynamics of Turing patterns under spatiotemporal forcing, *Phys. Rev. Lett.* **90** (2003) #128301, **doi:** 10.1103/PhysRevLett.90.128301.

[13] S. Touati, S. Lemita, M. Z. Aissaoui, Solving a nonlinear Volterra–Fredholm integro-differential equation with weakly singular kernels, *Fasc. Math.* **62** (2019) 155–168, **doi:** 10.21008/j.0044-4413.2019.0012.

[14] A. M. Turing, The chemical basis of morphogenesis, *Phil. Trans. Royal Soc. London B* **237** (1952) 37–72, **doi:** 10.1098/rstb.1952.0012.